

# Temporal variation in natural methane seep rate due to tides, Coal Oil Point area, California

J. R. Boles and J. F. Clark

Department of Geological Sciences, University of California, Santa Barbara, California, USA

I. Leifer

Department of Chemical Engineering, University of California, Santa Barbara, California, USA

L. Washburn

Department of Geography, University of California, Santa Barbara, California, USA

**Abstract.** Two large steel tents (each 30 m by 30 m), open at the bottom to the seafloor, capture  $\sim 16,800 \text{ m}^3 \text{ d}^{-1}$  (594 MCF) of primarily methane from a large natural hydrocarbon seep, occurring a kilometer offshore in 67 m of water. The gas is piped to shore where it is metered and processed. The seep flow rate was monitored hourly for 9 months. Our results show that the tidal forcing causes the flow rate to vary by 4–7% around the mean. These results are the first quantitative documentation of the effect of tides on natural gas seepage in relatively deep water. Time series analyses of the 9 month record clearly show four principal tidal components with periods of 12.0, 12.4, 23.9, and 25.8 hours. High tide correlates with reduced flow, and low tide correlates with increased flow. The correlation indicates that each meter increase of sea height results in a decrease of  $10\text{--}15 \text{ m}^3 \text{ hr}^{-1}$  or 1.5–2.2% of the hourly flow rate. The observed changes are best accounted for by a pore activation model, whereby gas is released from small pores at low pressures but is inhibited at higher pressure. Pressure-dependent gas solubility changes are a less likely cause of flow variation. Our study implies that sea level differences, on a tidal timescale, can significantly change the gas seepage rate from sediments. Lower sea level in the last hundred thousand years would presumably allow higher gas loss from the sediment, assuming sufficient gas present, because of reduced hydrostatic pressure at the sediment-sea interface. The magnitude of this long-term change cannot be extrapolated from our tidal data.

## 1. Introduction

Natural hydrocarbon seeps are found in varying intensity along most continental shelves [e.g., [Wilson et al.](#), 1974]. These seeps emit gas, oil, or a mixture of both from seafloor vents. During transit the gas dissolves, and depending on seepage rate and water depth, some of the hydrocarbon (gas and oil) reaches the surface where it accumulates as slicks and tar balls or is released into the atmosphere.

Marine hydrocarbon seeps are important local and regional sources of pollution. Seeps can be one of the largest sources of dissolved methane and larger hydrocarbon compounds in coastal environments [e.g., [Cline and Holmes](#), 1977; [Cynar and Yayanos](#), 1992; [Ward](#), 1992; [Radlinski and Leyk](#), 1995; [Clark et al.](#), 2000]. They are the most significant source of dissolved oil, surface oil slicks, and tar balls in some areas of the ocean [[Allen et al.](#), 1970; [Hartman and Hammond](#), 1981; [Whelan et al.](#), 1994; [MacDonald et al.](#), 1993; [Hornafius et al.](#), 1999].

Despite their importance as a natural pollution source, few studies of natural hydrocarbon seepage have quantified emission fluxes or temporal variability. A notable exception is the Coal Oil Point seep field, which is one of the largest known areas of active marine seepage. Several studies have quantified seep area [e.g., [Allen et al.](#), 1970; [Fischer and Stevenson](#), 1973], and others have quantified emission fluxes [e.g., [Hornafius et al.](#), 1999; [Quigley et al.](#), 1999; [Clark et al.](#), 2000].

Many processes can be postulated to explain short-term variations in seepage rates [e.g., [Hovland and Judd](#), 1988]. These include variation in seafloor pressure associated with tides, ocean swell, storm surges, bottom current velocities, and near-surface sediment hydrology. Seepage generally occurs through pores and fractures when gas pressures exceeds the sum of hydrostatic pressures, capillary pressures, and in some cases, sediment cohesion [e.g., [Judd and Sim](#), 1998].

Pore pressure changes induced by waves have been documented deep within sediments [[Okusa](#), 1985], showing the sensitivity of the system to changes in water height. Sufficiently long time series of seepage rates rarely exist to conclusively identify the effects of each of the postulated mechanisms. Variations in seepage due to tidal forcing have been documented in a number of shallow (<20 m) environments [[Mikolaj and Ampaya](#), 1973; [Bartlett et al.](#), 1988; [Chanton et al.](#), 2000]. Additional nontidal

Copyright 2001 by the American Geophysical Union.

Paper number 2000JC000774.

0148-0227/01/2000JC000774\$09.00

Reproduced by permission American Geophysical Union. Further reproduction or electronic distribution is not permitted.

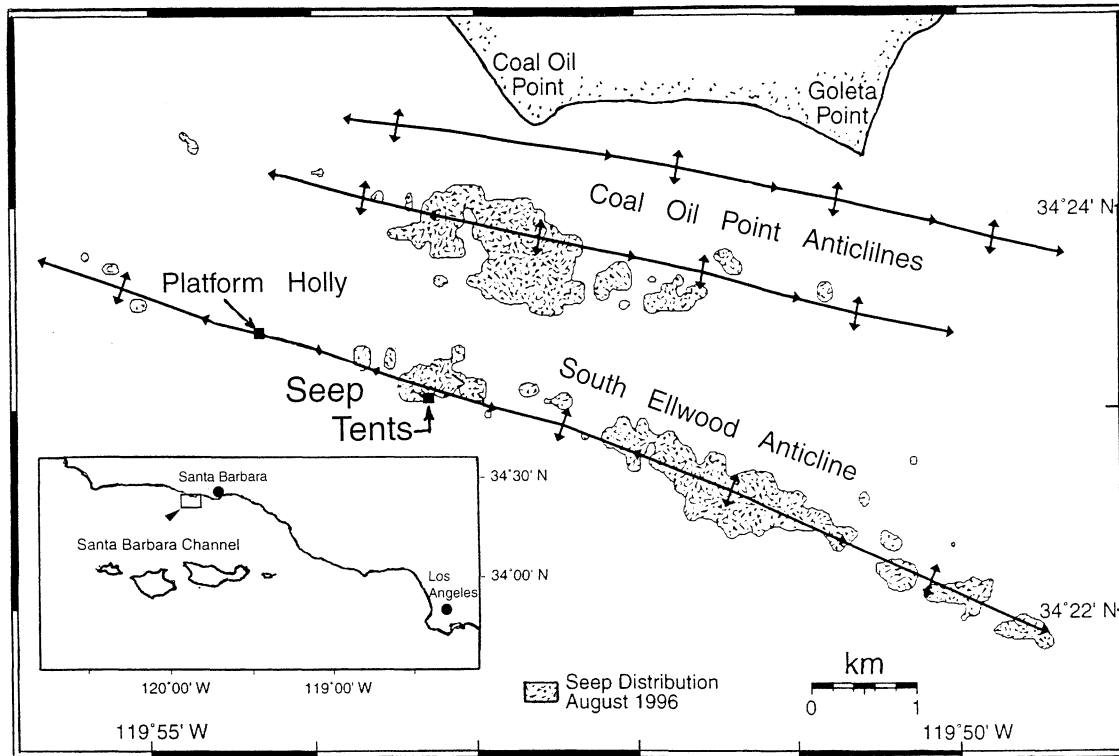


**Figure 1.** Map showing general location of hydrocarbon seepage around Coal Point, the seep tents, and Platform Holly [modified from Quigley et al., 1999]. The linear seep field extending southeast from Platform Holly (square) corresponds to a fault and the approximate axial crest of the Ellwood anticline [Christensen et al., 2000].

forcing was documented in a few seeps on Hydrate Ridge [Tryon et al., 1999]. In this setting, seepage rates are regulated by pore fluid and gas dynamics.

Here we present for the first time a high-quality time series of seepage rates from the Coal Oil Point seep field that allows us to examine hourly seepage variability and compare it with the hourly tide record. Subhourly pressure variations due to waves cannot be evaluated with our experiment, although our data will eventually allow monthly to yearly variability to be examined.

## 2. Gas Seeps in the Santa Barbara Channel

The northern margin of the Santa Barbara Channel is one of the most active areas of natural marine hydrocarbon seepage in the world [Hovland and Judd, 1988; Hornafius et al., 1999]. The most concentrated seepage area is found ~3 km offshore of Coal Oil Point, along the axis of the south Ellwood anticline. Significant hydrocarbon reserves are trapped within the anticline, and these have been produced at Platform Holly since 1964 (Figure 1). A northdipping fault with normal separation, parallel to the anticline axis, extends vertically ~1 km from the north edge of the reservoir to the sediment surface. Many seeps occur along this fault trace, indicating it is a permeable pathway [Christensen et al., 2000]. A parallel fault outcrops onshore near the coast. This fault has locally abundant methane-derived calcite cement [Boles and Grivetti, 2000]. Radiometric ages and isotopic composition of the calcite indicate methane seepage was active at least several hundred thousand years ago in the area.

Fischer and Stevenson [1973] noted changes in hydrocarbon seeps on decadal timescales in the Coal Oil Point area. They showed a marked drop in areas of seepage between 1946 and

1973 by comparing sonar data to oil company seep maps and attributed this drop to offshore production. During the last 6 years the UCSB seep group has mapped the seeps in the area using sonar images and quantified seepage flux from sonar and direct gas capture using a flux buoy [Washburn et al., 2001]. Results indicate that  $\sim 1.0 \times 10^5$  m<sup>3</sup>/d of seep gas is emitted from ~3 km<sup>2</sup> of the seafloor to the atmosphere [Hornafius et al., 1999; England, 2000]. An equal amount is injected into the coastal ocean [Clark et al., 2000]. Using data collected in 1973 and 1995, Quigley et al. [1999] demonstrated a decrease in the area and number of seeps within 1.5 km of Platform Holly, which they attributed to production from the platform.

## 3. Seep Tents

The seep was first visually observed on the sea surface, 1.6 km southeast from Platform Holly in 1970. The seep disappeared shortly thereafter and reappeared almost twice as active on June 4, 1973. The seafloor at this locality is in 67 m of water and consists of <5 m of Holocene sediment overlying Pleistocene strata. In September of 1982, the Atlantic Richfield Company (ARCO) installed two structures on the seafloor to capture hydrocarbons (Figure 2) [Rintoul, 1982]. The two tents, hereafter referred to as the seep tents, are steel pyramids with a total basal area of 1860 m<sup>2</sup> each weighing  $>3.18 \times 10^5$  kg (350 tons). The seep tents are anchored on the seafloor to 12 concrete blocks, each weighing  $2.27 \times 10^5$  kg (25 tons). In 1986, additional 450 m<sup>2</sup> skirts were added to the tent area. The seep tents have relief ports at ~3-4 m above the seafloor to prevent the gas from filling and lifting the tents if the flow line to shore became blocked. The tubular base

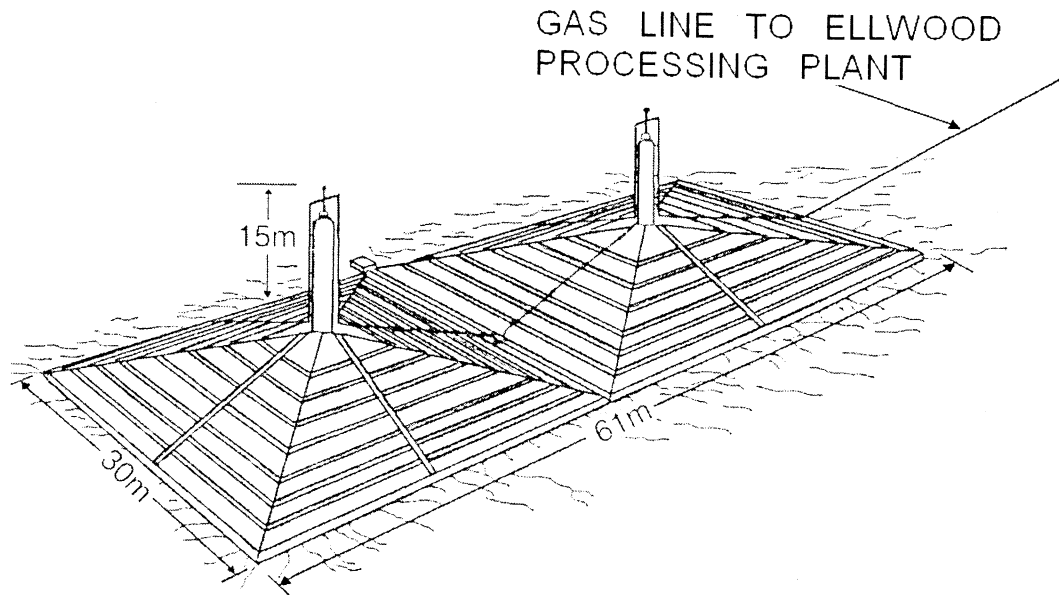


**Figure 2.** Diagram of seep tents installed by ARCO in 1982 off Coal Oil Point, California (modified from Reynolds, [1983]). The tents only partially cover a major seep complex, which erupted in 1973. Gas bubbles from the sediment through the water in the tent and accumulates at the top. A small gap between the roof and the base frame limits the amount of cross flow through the tent (see text). The captured gas flows through the gas line to the Venoco's Ellwood processing plant, where it is continuously monitored.

frame of each tent rests on the seafloor with a 50 cm gap between the frame and the lower edge of the tent roofs.

Seep gas is continually collected and piped onshore via a 15 cm diameter steel pipe, where it is monitored on an hourly basis and processed at the Ellwood plant (seep tents, Platform Holly, and plant are currently owned by Venoco). At the present seepage rates the gas transits through the tents and transfer pipe in ~15 min. On shore the back pressure in the flow line is regulated to  $5.6 \times 10^5$  Pa. This prevents seawater from being drawn into the transfer pipe at the top of the tent and regulates the height of the gas-water interface inside the tent. The mean pressure on the seafloor at 67 m is presumably hydrostatic ( $\sim 7 \times 10^5$  Pa). The back pressure in the flow line, once set, has no effect on variations in gas flow from the tents.

In August of 1982 the seafloor vents were located with manned submersible submarines and later mapped from a remote operated vehicle (ROV) using a preassembled grid on the seafloor for reference. More than 100 seafloor vents were mapped in the area of the tent sites (Figure 3a). Two years after installation of the seep tents in September of 1984, the seafloor was again mapped by ROV, but location accuracy was improved by placing acoustic beacons on a corner of the tent structure and the ROV (Figure 3b). Mapping extended for a distance of 50 m from the tents. The second survey showed new seeps around the periphery of the tents.

The change in seep locations may be due to the load of the seep tents on the seafloor, or the change may be natural. The appearance of new vents outside of the tents cannot be caused by back pressure on the seafloor beneath the tent. The relief ports, located below the gas-water interface, would prevent any back pressure from occurring. Figure 3 indicates that the position of seafloor vents can vary on timescales of order 2 years, although in this case the tents themselves may have caused the changes. Regardless of cause, long-term temporal changes of flow recorded at

the seep tents, which are fixed in space, may result from migration of active vent locations.

#### 4. Gas Flow Data

Gas flow data was obtained from a Total Flow Gas Monitoring System (Total Flow, Tulsa, Oklahoma) located at the Ellwood processing plant, just onshore from the seep tents. Temperature of the flow stream at the meter, static pressure of the flow stream on the downstream side of the meter, and differential pressure across the meter are recorded. From these data and gas specific gravity the instrument calculates hourly mean flow rate by averaging instantaneous measurements collected every 5 s. The recorded flow volume is standardized to 15.6°C and  $9.7 \times 10^4$  Pa. Earlier data (prior to 1994) for the seep tents were computed as an hourly flow rate from a pressure difference across a valve. These data were recorded at the same time each morning and extrapolated to a daily flow rate.

Initial gas capture in late 1982 was  $9 \times 10^5$  m<sup>3</sup> gas/month ( $5 \times 10^5$  m<sup>3</sup> barrel equivalent per month) (Figure 4a). Cumulative net oil production (emulsion) from the tent between September 1982 and June 1987 was 600 barrels (bbl) of 20-25 American Petroleum Institute (API) gravity crude; however, no oil has been collected since 1994. Addition of the tent skirts in 1986 increased gas capture by  $\sim 3 \times 10^5$  m<sup>3</sup> gas/month ( $1.5 \times 10^5$  m<sup>3</sup> barrel equivalent month), and capture reached a peak of  $\sim 1.4 \times 10^6$  m<sup>3</sup> gas/month ( $7.5 \times 10^5$  m<sup>3</sup> barrel equivalent/month) between 1986 and 1989 (Figure 4a). The seep rate then slowly declined to  $3 \times 10^5$  m<sup>3</sup> gas/month between 1990 and mid-1994, and since then, it has shown a slow but systematic increase to a present rate of  $5 \times 10^5$  m<sup>3</sup> gas/month [Quigley et al., 1999]. Our records extend the Quigley et al. daily data set from 1997 to 2000. Since about 1987, the hydrocarbon production trends (oil plus gas) from Platform

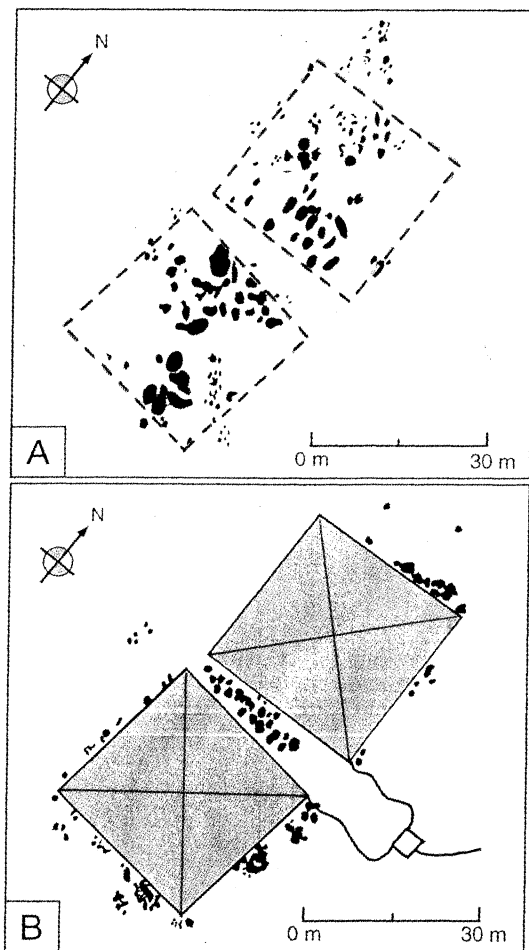


**Figure 3.** Map view of bubble sources (black spots) and seep tents on seafloor in 67 m of water. Maps are based on a remote operated vehicle (ROV) working on a preassembled wire grid placed upon the seafloor (Figure 3a) or ROV working from a radio beacon on the seafloor (Figure 3b). (a) Map (August 1982) of original seep localities prior to installation of the seep tents (shown as dashed lines). (b) Map (September 1984) of sea bottom 2 years after tents were installed. Note new bubble sources (black spots) that have formed around the edges of the seep tents (shaded area). Data are from ARCO files.

Holly are similar to trends of gas discharge from the seep tent (Figure 4a).

Our hourly flow record spans ~9 months, beginning August 31, 1999, and continuing through June 1, 2000 (Figure 4b). The gaps in the record represent intervals in which flow dropped owing to maintenance of the flow system. This record contains two long-term cycles, with a period of ~5 months, peaking at about October 1999 and March 2000. It is important to note that the seep rate has varied by a factor of 3 over the 17 year collection period. Superimposed on these large-scale and long-term changes are small but systematic variations, some of which are related to tide height.

## 5. Tidal Data

Tidal data for the seep area are based on predictions from commercial software Tides and Currents for Windows, version 2.5b (Nautical Software, Inc.) that uses National Oceanic and Atmospheric Administration (NOAA) data for the Santa Barbara

area. We have verified the tide predictions by collecting a time series of ocean pressure data at Platform Holly. A SBE Model 39 temperature/pressure recorder was attached to the leg of Platform Holly at 13 m below mean sea level for 3 weeks (July 7 to August 1, 2000). The instrument recorded the instantaneous pressure and temperature every 10 s. Both the pressure data and the predicted tide height data sets were normalized after the mean was subtracted to zero-center the data. Correlation coefficients were calculated for time-shifted (offset) pressure data. The best correlation ( $R^2=0.99$ ) is with zero time offset between data sets, the correlation decreasing with either longer or shorter time shifts. Thus the tide program predicted tide height to within  $\pm 10$  s of the measured height.

The tide height variation in the vicinity of the seep tent are relatively small. The average tide height in the area is  $\sim 0.85$  m (the tide datum is the average of the lower low water height of each tidal day observed over the National Tidal Datum Epoch). The average difference between high and low tide is  $\sim 1.1$  m. The maximum tidal range during the study period is  $\sim 2.5$  m.

## 6. Analysis of Gas Flow Time Series Data

We computed power spectrum of the flow rate  $q$  time series from the seep tents to examine the timescales of variability in the record. The  $\sim 6700$  hour record was first examined for data gaps and times when the flowmeter was being serviced. The latter were identified by very low or very high hourly flow rates, and these often occurred just before or just after longer data gaps. Inspection of the  $q$  time series showed that  $q$  fell in the range  $(1.5-1.7) \times 10^4$   $\text{m}^3/\text{d}$  when the flowmeter was operating correctly; values outside this range were excluded from the analysis. Bad data points and data gaps, accounting for  $\sim 12\%$  of the record, were replaced by the mean value of  $q$  computed from the remaining data points.

After substituting for missing or bad data, time series were divided into ensembles, either 512 or 2048 hours long, depending on the spectral resolution. Ensembles were tapered with a Han-

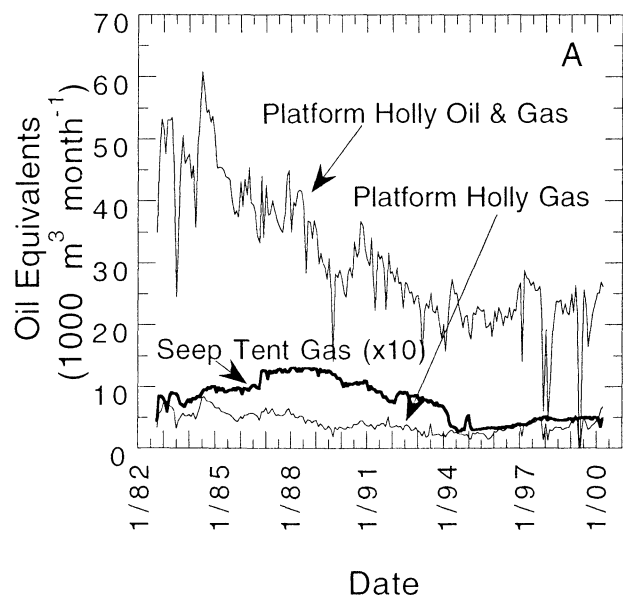


**Figure 4a.** Monthly gas flow from the seep tents and production from nearby Platform Holly for the period January 1, 1994, through August 31, 1999. Units are oil and British Thermal Unit (BTU) gas equivalents in  $\text{m}^3$  of liquid/month.

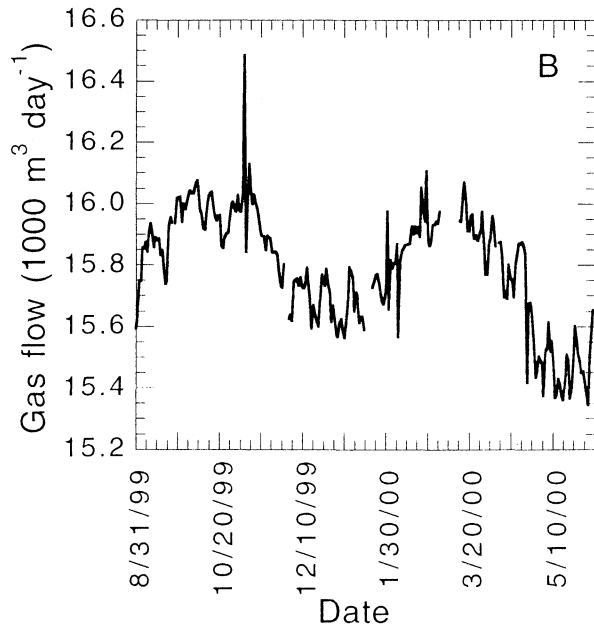


Figure 4b. Daily gas flow in  $10^3 \text{ m}^3$  of gas/d from the seep tents for the hourly monitoring period August 31, 1999, through June 30, 2000. Gaps in record are intervals in which the meter was shut down because of maintenance and repair.

ning window and then transformed via a fast Fourier transform (FFT) algorithm. Autospectra were estimated by averaging the FFTs from all the ensembles.

## 7. Results

For frequencies  $f$  less than  $\sim 0.7$  cycles per day (cpd) the spectral amplitude of  $q$  decreased strongly with  $f$  (Figure 5a). At higher  $f$  the amplitude was approximately white, except for 2 bands where strong peaks were evident, one at  $\sim 1$  cpd and the other at  $\sim 2$  cpd. These peaks, corresponding to the diurnal and semidiurnal tidal components, were the only significant sinusoids present based on the 95% confidence limits (vertical bar, Figure 5a). The transform length (512) was selected to maximize degrees of freedom in estimating spectral levels, while still resolving the dominant tidal components. It also verified that no sinusoids were present at other resolved frequencies. The corresponding spectral resolution was  $f = 0.048$  cpd.

To examine the region around the spectral peaks in more detail, the transform length was increased to 2048 points with a spectral resolution of  $f = 0.012$  cpd. The resulting spectral levels were more variable, as shown by the larger 95% confidence limits, but the increased resolution split the diurnal and semidiurnal peaks into two pairs of peaks (Figure 5b). Within the time series resolution the center frequencies of these peaks corresponded to the four dominant tidal constituents:  $O_1$  with a period 25.8 hours,  $K_1$  with a period of 23.9 hours,  $M_2$  with a period of 12.4 hours, and  $S_2$  with a period of 12.0 hours, (Figure 5b)[e.g., Pond and Pickard, 1983]. All four peaks were well resolved, exceeding the surrounding spectral levels by at an order of magnitude or more.

In order to quantify the effect of changing tide height on gas capture, three 6 day time intervals were picked that showed particularly large differences between high and low tide. The intervals were November 21–26, 1999, December 20–25, 1999, and February 16–21, 2000. These segments have average calculated

tidal differences of  $>1.5$  m (average tidal difference for the entire study period is 1.1 m).

In each of the three intervals, high tide correlated with low flow rate, and low tide correlated with high flow (e.g., Figure 6a). The regression coefficient  $R^2$  was between 0.50 and 0.53 for the three intervals.

In Figure 6b, flow rate is plotted against peak tide changes using the data set for December 20–25, 1999. Each flow rate value is the mean of the peak and the two adjacent points at peak tide change. These average flow rates were plotted because some records have small hourly spikes in flow rate and peak tide events can extend over several hours. For this analysis,  $R^2 = 0.85$  and is considerably better than that on the entire hourly data set for this time series (Figure 6a). Similar plots for the other time series yielded  $R^2 = 0.83$  for November 21–26, 1999, and  $R^2 = 0.81$  for February 16–21, 2000. This suggests that the flow at the time of peak tide changes is more closely related to the tide height than during the overall time period. For every meter increase in tide height, the flow rate decreased between 10 and 15  $\text{m}^3/\text{h}$ . Each additional meter of sea height represents a pressure increase of  $\sim 10^4$  Pa. The tidal affect causes the flow to vary 4–7% around the mean flow (i.e., up to 50  $\text{m}^3/\text{h}$  variation for flows of 630–680  $\text{m}^3/\text{h}$ ).

Correlation coefficients were also calculated for time shifted (offset) flow data against tide height using the data set for December 20–25, 1999 (Figure 7). The best fit between plots of flow versus tide height is with zero time offset. In other words the peak flow corresponds best to the peak tidal events (within the one hour resolution of the data set).

The long-term ( $\sim 5$  months) cyclic variation in flow from the seep tents (Figure 4b) does not appear to be directly related to tides. The average tide height during the peak flow intervals of September 28 to November 9, 1999, and February 15 to March 28, 2000, were 89 and 79 cm, respectively. The two low-flow portions of the cycle, December 7, 1999, through January 4, 2000, and April 25 to June 14, 2000, have mean tide heights of 84 and 79 cm, respectively. Thus this long-term cyclic change in flow rate does not correlate with changes in mean tide height. We are continuing to collect data from the seep tents to determine if these cycles are characteristic of the flow record.

## 8. Discussion

### 8.1. Proposed Physical Models of Tide Height

#### Influence on Seepage Rate

**8.1.1. General considerations.** Natural gas escapes from subsurface reservoirs through fractures and pores in the sedimentary rocks as a mixture of free gas, dissolved gas, oil, and water. Observation of seeps away from the tents have shown that large seeps modify the local environment by generating very strong upwelling flows, by turbulence, and by saturating the water contained within the bubble plume with methane [Leifer et al., 2000]. Presumably, some of these effects also occur within the seep tents.

Within the seep tents the bubbles rise from the seafloor vents through the water column for a distance of  $\sim 6$  m before they accumulate in the gas cap. Circulation between ambient ocean water and the tent water must be very restricted as a result of the narrow ( $\sim 50$  cm) gap between the tent roof and the tubing frame that is on the seafloor. Once the rising bubble stream is established, there is no effective way for seawater to circulate into and

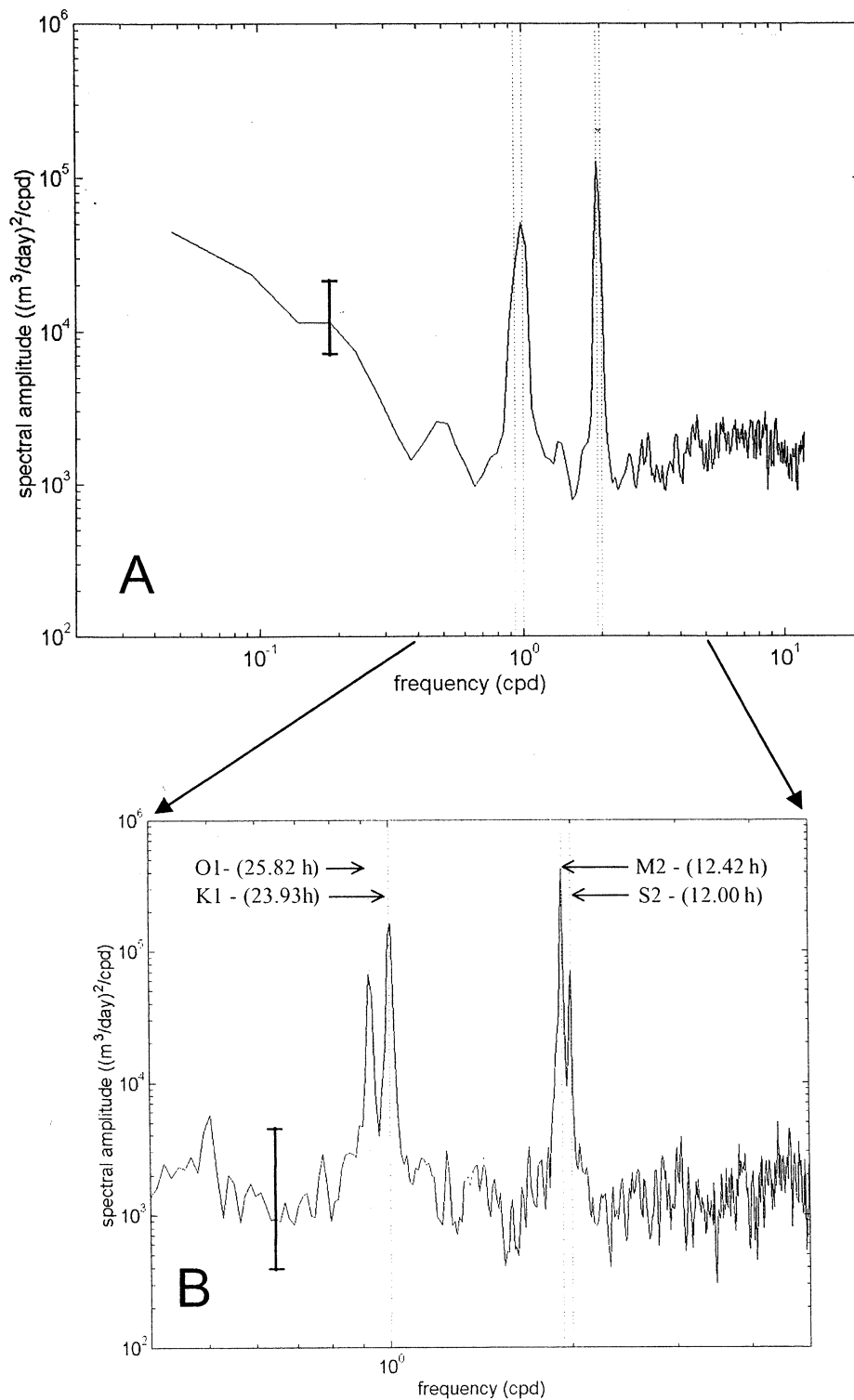


**Figure 5.** (a) Autospectrum of seepage rate  $q$  from period August 31, 1999 to June 30, 2000. Strong peaks at 1 and 2 cpd corresponded to diurnal and semidiurnal tidal components. Vertical bar indicates 95% confidence limits. (b) As in Figure 5a, but frequency axis has been expanded and spectrum was computed with 4 times the spectral resolution. The peaks of Figure 5a split into two pairs of peaks corresponding to the O<sub>1</sub> and K<sub>1</sub> diurnal components and the M<sub>2</sub> and S<sub>2</sub> semidiurnal components. Frequencies of these four tidal components are indicated by vertical dotted lines in both Figures 5a and 5b.

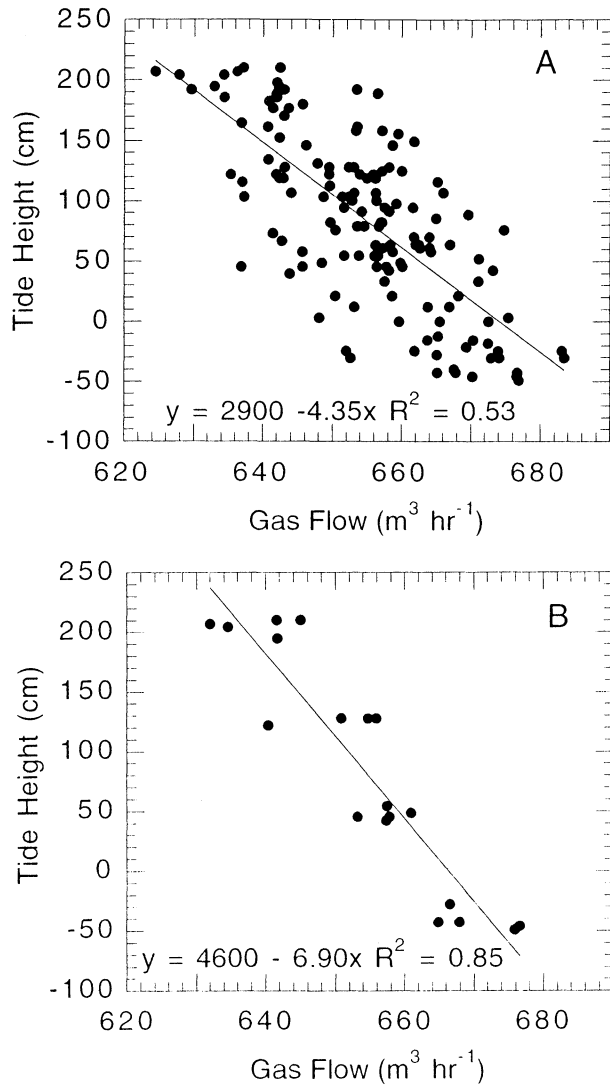


**Figure 6.** Comparison of gas flow rate from the seep tents with tide height for the period December 20-25, 1999. Tide height is the average for the hour in which the flow rate is recorded and is estimated from the Tides and Currents program (see text). (a) Comparison of hourly flow rate to tide height at each hour of the time period. Note that an increase in tide height corresponds to a decrease in flow rate. (b) Comparison of the seep tents flow with peak tide changes for the period December 20-25, 1999. Each flow rate is the average of three hourly values around the tide change. This plot suggests that the periods of changing tide are more closely correlated with gas flow than the entire hourly data set for this time period (Figure 6a).

out of the tent; however, circulation of trapped water within the tent should be vigorous. Restricted circulation of seawater into or through the tent would limit the likely explanations for our observations. Hence the influence of tidal currents and pressure-related changes in gas solubility should be reduced by the artificial environment of the seep tents.

The time series data show that the seepage rate decreased with increasing tidal height, and spectral analysis clearly shows tidal cycle frequencies. Several potential mechanisms could explain variability in gas emission rate due to the tidal cycle, which must result from changes in the hydrostatic pressure  $P_H$ , defined

$$P_H = \rho g z + P_A, \quad (1)$$

where  $\rho$  is the water density,  $g$  is gravity,  $z$  is the water depth, and  $P_A$  is the atmospheric pressure. These mechanisms include a combination of  $P_H$  induced changes in pore throat activation and gas saturation. As discussed below, the pore throat activation mechanism is most likely dominant.

**8.1.2. Pore throat activation.** An important process that can explain the variability in flow rate as a function of tide height is the pressure effect on gas escaping from a range of pore and fracture throat sizes [Blanchard and Syzdek, 1977; Longuet-Higgins et al., 1991]. Brown [2000] demonstrates from theoretical and observed migration rates that gas is transferred as a continuous phase from leaking reservoirs, rather than as isolated colloidal size bubbles. We envision that the gas is moving from the reservoir along the fault and fracture pathway as gas slugs of varying size and these are continuously escaping from the seafloor.

Owing to viscous forces on the slugs of gas within the fractures the fracture pressure  $P_F$ , a nonequilibrium pressure from gas flow, decreases from the reservoir until the point where bubbles are released. The pressure in the growing bubble  $P_B$  is the sum of  $P_{ST}$ , the surface tension (i.e., Laplace pressure), and  $P_F$  at the pore and fracture throat. For a bubble to form within the sediment or rock near the seafloor,  $P_F + P_{ST}$  must be greater than  $P_H$ . If not, water will penetrate into the pore and fracture to a depth where  $P_H = P_F + P_{ST}$ . The emitted bubble size scales with throat size, and the smaller the throat, the more energy (pressure) is required to overcome the capillary pressure [Blanchard and Syzdek, 1977].

As each bubble is released, the pressure momentarily decreases until another bubble is produced. Since  $P_{ST}$  is inversely proportional to bubble radius  $r$ , larger bubbles are easier to produce, and of course, the release of a large bubble causes a greater decrease in  $P_F$ . As a result, large bubbles are energetically preferred. In the simplest case, a single bubble size would be produced from a single throat size, and all other throats would be inactive. However, if, owing to the complex network of fractures, the bubble release does not reduce the pressure sufficiently in neighboring throats, smaller throats can also be activated. Because of the inverse relationship between  $P_{ST}$  and  $r$ , there is a

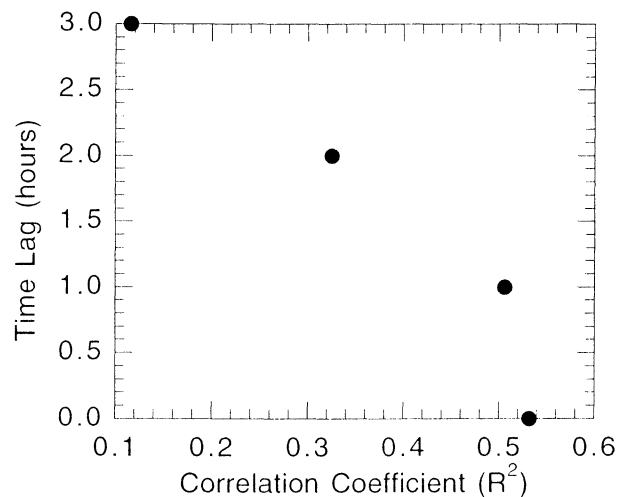


**Figure 7.** Correlation coefficient ( $R^2$ ) between seep tents flow rate and tide height as a result of hourly time offset of flow data relative to tide height data (data set for the period December 20-25, 1999). Plot shows that little if any lag occurs between change in tide height and flow conditions.

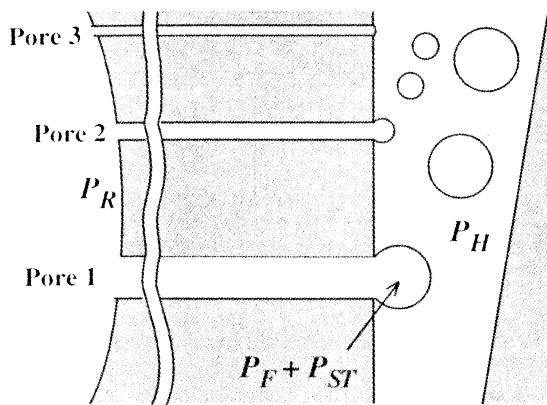


**Figure 8.** Schematic representation of pore activation model.  $P_R$  is pressure in reservoir,  $P_F$  is pressure in fracture,  $P_{ST}$  is surface tension pressure, and  $P_H$  is hydrostatic pressure.

critical size for which smaller throats do not produce any bubbles. This situation is shown schematically in Figure 8, where most of the gas (and the largest bubbles) is released by the largest throat (pore 1). Gas is also released at smaller throats (pore 2), which are larger than some critical size where no bubbles are produced (pore 3).

The pore throat activation model of seepage works in this fashion. A tidally induced drop in  $P_H$  allows more throats to be active and gas emission increases, whereas for an increase in  $P_H$ , fewer throats are active. Eventually, the increased flow due to a drop in  $P_H$  decreases  $P_F$ , and the system returns to equilibrium. An analogy is an aquarium air stone. Near the surface, a wide range of bubbles, including smaller bubbles, are produced, but as the stone is moved deeper, fewer of the small bubbles are produced.

In natural seeps, complex hydrologic flow systems often form as a result of the release of gas at the seafloor [O'Hara et al., 1995; Tyron et al., 1999]. Because bubbles in pores or fractures escape more easily in flowing pore water, any fluid motion will enhance emission rates and the ability of particular throats to remain active. Bubbles also escape more easily in the presence of bottom currents.

**8.1.3. Solubility.** The change in gas solubility with pressure could potentially explain the relation between tide height and  $q$ . The flux of gas captured by the seep tents does not precisely equal the flux of gas emitted from the vents because a fraction of the bubbles dissolve during the 6 m transit from the seafloor to the gas-water interface. We can describe this system by relating the seafloor seep flux  $q_{seep}$  to the flux into the seep tents  $q_{tent}$  and to the dissolution flux  $q_{ocean}$  by

$$q_{seep} = q_{ocean} + q_{tent} \quad (2)$$

The gas dissolution rate into the ocean  $q_{ocean}$  varies because of pressure changes since bubble outflow is driven by the difference between the oceanic aqueous concentration  $C$  and the bubble equivalent concentration  $C_{eq}$ , which is dependent on hydrostatic pressure and solubility. Increased bubble dissolution in the tent water results in less gas reaching the gas-water interface and a decrease in  $q_{tent}$ .

An estimation of the timescale to establish equilibrium between the bubble partial pressure and the aqueous concentration is presented in Appendix A. An equilibration time of 580 s is

calculated for a 3% pressure change (due to tide height) assuming (1) the total gas flow is  $0.2 \text{ m}^3/\text{s}$ , (2) the total seep tents volume is  $3900 \text{ m}^3$ , (3) the bubble radius is  $1000 \mu\text{m}$ , (4) bubbles are free of oil [Patro et al., 2000], (5) the bubbles equilibrate during their rise through the water in the seep tent, and (6) the exchange of water in and out of the seep tents is very small. Once equilibrium is reached, transfer of gas between bubbles and water stops (i.e.,  $q_{ocean} = 0$ ).

In equilibrium the water within the seep tents contains  $\sim 1000 \text{ m}^3$  of dissolved methane at STP. Seafloor pressures during high tide are  $\sim 3\%$  larger than during low tide (these would be relative extreme values). Hence, between each high and low tide the amount of dissolved methane will fluctuate by  $\pm 15 \text{ m}^3$  at STP. To achieve the necessary tidal change,  $q_{ocean}$  must average  $0.0014 \text{ m}^3/\text{s}$  into the water during the rising tide and  $0.0014 \text{ m}^3/\text{s}$  out of the water during the falling tide. Thus the tidal change in  $q_{ocean}$  is  $0.0028 \text{ m}^3/\text{s}$  or  $<1.5\%$  of the mean flux into the seep tent ( $q_{tent}$ ). Because the observed change in  $q_{tent}$  is 4-7%, this suggests that solubility changes are not dominant.

## 8.2. Effect of Pressure Changes on Flow

An earlier study reported a decrease in oil seepage rate associated with an increasing tide height in the Coal Oil Point area [Mikolaj and Ampaya, 1973]. This study was based on oil captured in small plastic bags positioned over several small oil seeps at  $\sim 15\text{-}18 \text{ m}$  depth during several 3-5 hour time periods. They observed a negative correlation between oil seep rate and tide height, similar to our findings on variations in gas flow rate with tide height. These oil seeps are apparently much more sensitive to pressure changes as they report 20-30% changes in seepage rate with the tide, perhaps due to the shallow depth of the seeps or the higher viscosity of the oil.

Results of our study indicate that the seepage rate from ocean sediments is closely balanced with the height of the overlying water over short timescales. This response may be related to the structure of the gas pathways in the shallow sediments. Over longer timescales the shallow system recharge rate by the deeper reservoir should be important.

Presumably, large-scale changes in sea level could have a marked effect on the amount of gas escaping from marine sediments. Large decreases in sea level could lead to substantial amounts of methane released to the atmosphere if sufficient gas were available. Sea level has varied by  $>100 \text{ m}$  during the past few hundred thousand years in response to the glacial cycle [Rohling et al., 1998]. Although these large-scale sea level changes may have initially caused significant increases in seepage rates, the response over longer timescales would be determined by the supply of gas from deeper reservoir to the surface. With time the seafloor seeps would reach a flow rate controlled by a balance between gas production, reservoir pressure, and pathway permeability. Although the magnitude of the effect of long-term sea level changes cannot be extrapolated from either our data or our model, a drop in pressure due to lower sea level would presumably increase the gas seepage at some scale. This is a separate effect from the hypothesis that a pressure drop due to falling sea level could destabilize methane clathrates [MacDonald, 1990; Nisbet, 1990; Kennett et al., 2000].

## Appendix A

The value of  $q_{ocean}$  varies because  $P_H$  changes since it is the difference between oceanic aqueous concentration  $C$  and bubble

equivalent concentration  $C_{eq}$  that drives bubble outflow.  $C_{eq}$  is calculated from Henry's Law [Lincoff and Gossett, 1984] and the bubble pressure  $P_B$ ,

$$C_{eq} = HP_B, \quad (A1)$$

where  $P_B$  is given by

$$P_B = P_H + \frac{2\sigma}{r}, \quad (A2)$$

where  $P_H$  is the hydrostatic pressure and  $2\sigma/r$  is the La Place pressure due to surface tension  $\sigma$  and  $r$  is the bubble radius. The La Place pressure is negligible relative to  $P_H$  except for the very smallest bubbles at the shallowest depths (e.g., for  $r = 50 \mu\text{m}$ ,  $2\sigma/r \sim 0.03 \text{ atm}$ , or 3% of  $P_H$  for 10 m).

The bubble gas outflow, or flux  $q$ , is given by the individual gas bubble flux equation,

$$\Gamma = \frac{dn}{dt} = 4\pi r^2 k_B (C - HP_B), \quad (A3)$$

where  $n$  is the bubble molar content,  $t$  is time, and  $k_B$  is the individual bubble gas transfer rate.

The total seep ( $q_{ocean}$ ) is determined by integrating the number of bubbles of each size class over the path (i.e., from emission to collection or the surface) of each bubble. While in equilibrium  $q_{ocean} = 0$ ; tidal changes in  $P_H$  cause disequilibrium for the bubbles,  $q_{ocean} \neq 0$ . Because of  $q_{ocean}$ ,  $C$  asymptotically approaches  $HP_B$ , but as a result of  $q_{ocean}$ ,  $q_{atmosphere}$  is greater (or less). Implicit is the assumption that the seep plume water is not well mixed with the ocean (i.e., the timescale for  $C$  to change due to bubble gas flux is shorter than the mixing timescale between the bubble plume and the ocean). To estimate the seep tent timescale  $\tau_{ST}$ , which is due to  $q_{ocean}$ ,  $q$  for the bubbles needs to be estimated. The simplest approach is to determine if the bubbles equilibrate and, if so, assume that  $q = n$ .

Assuming constant  $r$ , the bubble equilibration timescale  $\tau_e$  can be calculated by solving (3) and using the ideal gas law

$$PV = nRT, \quad (A4)$$

where  $R$  is the universal gas constant,  $T$  is the temperature, and  $V$  is the bubble volume ( $V = 4/3 \pi r^3$ ). This yields [Woolf and Thorpe, 1991],

$$\tau_e = \frac{r}{3k_B} \frac{H}{RT}, \quad (A5)$$

Using (5) for  $\text{CH}_4$ ,  $\tau_e$  for 500, 1000, and 5000  $\mu\text{m}$  bubbles is 13, 22, and 270 s, respectively (15°C, clean). Since bubbles larger than  $\sim 500 \mu\text{m}$  rise at 0.2 m/s to 0.3 m/s, this is a rise time of 20-30 s for the seep tent's 6.3 m height. Thus, for a well-mixed rise path a bubble of  $\sim 1000 \mu\text{m}$  will equilibrate during the rise. Since the water will always be near equilibrium and needs only adjust to tidal  $P_H$  variations  $\sim 2 \text{ m}$ , or 3%,  $\tau_{ST}$  is 580 s.

This calculation is very rough, as  $\tau_{ST}$  should be calculated by solving the equation for  $dC/dt$ . Furthermore,  $\tau$  is certainly less since an equilibrated bubble only transfers  $(1 - e^{-1})$  of its  $\text{CH}_4$ . Furthermore, while upwelling flows in the seep tents decrease the transfer time and the amount of bubble equilibration may not equilibrate, oil contamination may increase  $\tau_{ST}$ . Alternatively, bubble-generated turbulence will increase  $q$ .

Since the bubbles equilibrate, we can use the simplifying assumption that the entire bubble's  $\text{CH}_4$  enters the tent water and calculate a timescale for the seep tent water to equilibrate from an initial condition with no gas. Gas flux for the two seep tents is 0.2  $\text{m}^3/\text{s}$  at STP. Assuming  $r$  is 1000  $\mu\text{m}$  for all bubbles, this is  $4.5 \times 10^7$  bubbles/s. Each seep tent has a volume of 1950  $\text{m}^3$  (volume ( $\text{m}^3$ ) =  $AH/3 = 30.5 \times 30.5 \times 6.3/3$ ). Using  $H = 7.9 \times 10^5$

atm per mol per  $\text{cm}^{-3}$  for  $\text{CH}_4$ , at a depth of 66 m, or  $P = 7.6 \text{ atm}$ ,  $C_{eq}$  is 9.62  $\text{mol}/\text{m}^3$ , or a total of  $1.9 \times 10^4 \text{ mol}$ . The 0.1  $\text{m}^3/\text{s}$   $\text{CH}_4$  flux per seep tent at STP is equal to  $\sim 1.0 \text{ mol}/\text{s}$ . Thus  $\sim 5.2$  hours is required to completely saturate the seep tent water.

**Acknowledgments.** We acknowledge the assistance of Venoco in all aspects of data collection and discussions of the tent and gas production. Karen Christensen, John Dimizio, Chris Knight, and Bob Van Nostrand Jr. have been particularly helpful. Don Stamp, ABS systems, has been very helpful in downloading the gas flow data. Paul Rowley, retired ARCO offshore superintendent, has been very helpful providing historical information on the seep tent. Discussions with Bruce Luyendyk, UCSB, regarding channel seeps have also been of great assistance. This work has been supported by University of California Energy Institute Grant (J. R. Boles and J. F. Clark) and DOE grant 444033-22433 (J. R. Boles G. Garven).

## References

- Allen, A. A., R. S. Schlueter, and P. G. Mikolaj, Natural oil seepage at Coal Oil Point, Santa Barbara, California, *Science*, 170, 974-977, 1970.
- Bartlett, K. B., P. M. Crill, S. A. Bonass, J. E. Richey, and R. C. Hariss, Wet season methane emissions from the Amazon floodplain, *Eos Trans. AGU*, 69, 320, 1988.
- Blanchard, D. C., and L. D. Syzdek, Production of air bubbles of a specified size, *Chem. Eng. Sci.*, 32(9), 1109-1112, 1977.
- Boles, J. R., and M. Grivetti, Calcite cementation along the Refugio/Careros fault, coastal California: A link between deformation, fluid movement and fluid-rock interaction at a basin margin, *J. Geochem. Explor.*, 69-70, 313-316, 2000.
- Brown, A., Evaluation of possible gas microseepage mechanisms, *AAPG Bull.*, 84, 1775-1790, 2000.
- Chanton, J. P., C.S. Martens, and C. A. Kelley, Gas transport from methane-saturated, tidal freshwater and wetland sediments, *Limnol. Oceanogr.*, 34, 807-819, 2000.
- Christensen, K. I., M. D. Wracher, and G. A. Orr, South Ellwood Field, Santa Barbara Channel: New Insight into structures, fractures and seeps, paper presented at AAPG Pacific Section Meeting, Am. Assoc. of Petrol. Geol., Long Beach, Calif., 2000.
- Clark, J. F., L. Washburn, J. S. Hornafius, and B. P. Luyendyk, Dissolved hydrocarbon flux from natural marine seeps to the southern California Bight, *J. Geophys. Res.*, 105, 11,509-11,522, 2000.
- Cline, J. D., and M. L. Holmes, Submarine seepage of natural gas in Norton Sound, Alaska, *Science*, 198, 1149-1153, 1977.
- Cynar, F. J., and A. A. Yayanos, The distribution of methane in the upper waters of the Southern California Bight, *J. Geophys. Res.*, 97, 11,269-11,285, 1992.
- Egland, E. T., Direct capture of gaseous emissions from natural marine hydrocarbon seeps offshore of Coal Oil Point, Santa Barbara, California, M.A. thesis, 59 pp., Univ. of Calif., Santa Barbara, 2000.
- Fischer, P. J., and A. J. Stevenson, Natural Hydrocarbon seeps, Santa Barbara basin, California, in *Santa Barbara Channel Area Revisited Field Trip Guidebook*, vol. 3, edited by P. J. Fischer, pp. 17-28, Am. Assoc. of Petrol. Geol., Tulsa, Okla., 1973.
- Hartman, B. and D. Hammond, The use of carbon and sulfur isotopes as correlation parameters for the source identification of beach tar in the southern California borderland, *Geochemica et Cosmochemica Acta*, 45, 309-319, 1981.
- Hornafius, J. S., D. Quigley, and B. P. Luyendyk, The world's most spectacular marine hydrocarbon seeps (Coal Oil Point, Santa Barbara Channel, California): Quantification of emissions, *J. Geophys. Res.*, 104, 20,703-20,711, 1999.
- Hovland, M., and A. G. Judd, *Seabed Pockmarks and Seepages Impact on Geology, Biology, and the Marine Environment*, 293 pp., Graham and Trotman, London, 1988.
- Judd, J. G., and R. Sim., Shallow gas migration mechanisms in deep water sediment, in *Offshore Site Investigation and Foundation Behavior: New Frontiers*, edited by D. A. Arduis et al., pp. 163-174, Soc. of Underwater Technol., London, 1998.
- Kennett, J. P., K. G. Cannariato, I. L. Hendy, and R. J. Behl, Carbon isotopic evidence for methane hydrate instability during Quaternary interstadials, *Science*, 288, 128-133, 2000.

- Leifer, I., J. Clark, and R. Chen, Modifications of the local environment by a natural marine hydrocarbon seep, *Geophys. Res. Lett.*, 27, 3711-3714, 2000.
- Lincoff, A. H., and J. M. Gossett, The determination of Henry's constant for volatile organics by equilibrium partitioning in closed systems, in *Gas Transfer at Water Surfaces*, edited by W. Brutsaert, and G. H. Jirka, pp. 17-25, D. Reidel, Norwell, Mass., 1984.
- Longuet-Higgins, M. S., B. R. Kerman, and K. Lunde, Release of air bubbles from an underwater nozzle, *J. Fluid Mech.*, 230, 365-390, 1991.
- MacDonald, G. J., Role of methane clathrates in past and future climates. *Clim. Change*, 16, 247-281, 1990.
- MacDonald, I. R., N. L. Guinasso Jr., S. G. Ackleson, J. F. Amos, R. Duckworth, R. Sassen, and J. M. Brooks, Natural oil slicks in the Gulf of Mexico visible from space, *J. Geophys. Res.*, 98, 16,351-16,364, 1993.
- Mikolaj, P. G. and J. P. Ampaya, Tidal effects on the activity of natural submarine oil seeps, *Marine Technical Society Journal*, 7, 25-28, 1973.
- Nisbet, E.G., Climate change and methane, *Nature*, 347, 2001, 1990.
- Okusa, S., Measurements of wave-induced pore pressure in submarine sediments under various marine conditions, *Mar. Geotechnol.*, 6, 119-144, 1985.
- O'Hara, S. C. M., P. R. Dando, U. Shuster, A. Bennis, J. D. Boyle, F. T. W. Chui, T. V. J. Hatherell, S. J. Niven, and L. J. Taylor, Gas seep induced interstitial water circulation: Observations and environmental implications, *Conti. Shelf Res.*, 15, 931-948, 1995.
- Pond, S., and G. E. Pickeard, *Introductory Dynamical Oceanography*, 2nd ed., 329 pp., Pergamon, New York, 1983.
- Quigley, D. C., J. S. Hornafius, B. P. Luyendyk, R. D. Francis, J. Clark, and L. Washburn, Decrease in natural marine hydrocarbon seepage near Coal Oil Point, associated with offshore oil production, *Geology*, 27, 1047-1050, 1999.
- Radlinski, A. P., and Z. Leyk, Formation of light-hydrocarbon anomalies in ocean waters, *Geology*, 23, 265-268, 1995.
- Reynolds, A., ARCO seep capture, *Manzingira*, 7, 56-65, 1983.
- Rintoul, B., ARCO caps Santa Barbara channel seep, *Pac. World Oil*, 74, 6-9, 1982.
- Rohling, E. J., M. Fenton, F. J. Jorissen, P. Bertrand, G. Ganssen, and J. P. Caulet, Magnitudes of sea-level lowstands of the past 500,000 years, *Nature*, 394, 162-165, 1998.
- Tryon, M. D., K. Brown, M. E. Torres, M. Tréhu, J. McManus, and R. W. Collier, Measurements of transience and downward fluid flow near episodic methane gas vents, Hydrate Ridge, Cascadia, *Geology*, 27, 1075-1078, 1999.
- Ward, B. B., The subsurface methane maximum in the California Bight, *Cont. Shelf Res.*, 12, 735-752, 1992.
- Washburn, L. C., C. G. Johnson, C. C. Gotschalk, and E. T. Eglund, A gas-capture buoy for measuring bubbling gas flux in oceans and lakes, *J. Atmos. Ocean. Technol.*, 18, 1411-1420, 2001.
- Whelan, J. K., M. C. Kennicutt II, J. M. Brooks, D. Schumacher, and L. B. Eglinton, Organic geochemical indicators of dynamic fluid flow processes in petroleum basins, *Org. Geochem.*, 22, 587-675, 1994.
- Wilson R. D., P. H. Monaghan, A. Osanik, L. C. Price, and M. A. Rogers, Natural marine oil seepage, *Science*, 184, 857-865, 1974.
- Wolf, D. K. and S. A. Thorpe, Bubbles and the air-sea exchange of gases in near saturation conditions. *J. Mar. Res.*, 49, 435-466, 1991.

---

J. R. Boles, University of California, Santa Barbara, Department of Geological Sciences, Santa Barbara, CA 93106. (boles@geo.ucsb.edu)

J. F. Clark, University of California, Santa Barbara, Geological Sciences & Environmental Studies Program, Santa Barbara, CA 93106. (clark@geol.ucsb.edu)

I. Leifer, University of California, Santa Barbara, Department of Chemical Engineering, Santa Barbara, CA 93106. (ira.leifer@bubbleology.com)

L. Washburn, University of California, Santa Barbara, Department of Geography, Santa Barbara, CA 93106. (washburn@icess.ucsb.edu)

(Received December 27, 2000; revised May 23, 2001; accepted July 16, 2001.)